Rotational interference in vibrational ladder climbing in NO by chirped infrared laser pulses

D. J. Maas,* M. J. J. Vrakking, and L. D. Noordam
FOM Institute for Atomic and Molecular Physics, Kruislaan 407, 1098 SJ Amsterdam, The Netherlands
(Received 6 October 1998; revised manuscript received 19 March 1999)

Results from experiments and model calculations on rotational interference in vibrational ladder climbing in the $X\ ^2\Pi_{1/2}$ state of NO are presented. In the low-fluence limit, the population in excited vibrational states shows an oscillatory behavior as a function of the chirp of the IR laser pulse. The interference is due to the accumulated phase difference of pathways involving different intermediate rotational states. The theoretical results match the experiments on an absolute scale. [S1050-2947(99)03808-1]

PACS number(s): 42.50.Hz, 42.65.Re, 41.60.Cr, 33.80.−b

I. INTRODUCTION

In studies of infrared multiphoton excitation and dissociation of polyatomic molecules a limiting factor is frequently the ability of a molecule to efficiently absorb the first few photons before it reaches a quasicontinuum of vibrational levels, e.g., [1–5]. This is largely due to the fact that molecular vibrations are anharmonic, so that the energy difference between successive vibrational levels decreases as one progresses up a vibrational ladder. Short-pulse laser excitation opens interesting new possibilities in this regard. The wide bandwidth of femtosecond laser pulses means that in principle photons for a number of successive transitions may simultaneously be present in a single femtosecond laser pulse, whereas the high power of modern laser systems means that multiple photon absorptions within a single pulse are possible. Furthermore, the spectral phase of femtosecond laser pulses can be manipulated. By applying a chirp to the pulse, for example, the instantaneous frequency of the laser can be adapted to the evolution of the molecule as it is pumped up the vibrational ladder [6–8].

In this paper we present results on the experimental observation of enhanced vibrational ladder climbing through the application of chirped laser pulses. Experimental results are presented which show that the efficiency of exciting the NO molecule from the $v''=0$ ground vibrational state to vibrational states $v'=2-4$ can be considerably enhanced by the application of a down-chirped laser pulse (i.e., a pulse where the instantaneous laser frequency decreases in time). At the same time, the experiments show the existence of an additional constraint on the transfer efficiency, which is due to interferences in the excitation between competing pathways connecting the same initial and final states. In earlier work [9,10] on chirped pulse excitation of Rb atoms, interferences in the transfer from the $5s$ ground state to the $5d$ excited state of Rb were observed due to competition between two-step resonant excitation and nonresonant two-photon excitation. While this same mechanism is active in the current experiment, we will show here that in a molecular system an even more important interference arises due to the availability of competing rotational pathways. For example, excitation to final state $|v=2,J''\rangle$ from initial state $|v''=0,J''\rangle$ is possible via intermediate states $|v'=1,J'=J''+1\rangle$, $|v'=1,J'=J''\rangle$, and $|v'=1,J'=J''-1\rangle$. The beating of all these independent contributions to the population transfer to excited rovibrational states of NO results in an oscillatory behavior as a function of the chirp. It will be shown that rotational interference explains the oscillatory behavior of the transfer efficiency to higher vibrational states as a function of the chirp of the excitation laser pulse.

The organization of this paper is as follows. In Sec. II we present the experimental results, showing a considerable chirp enhancement for down-chirped laser pulses as well as the occurrence of interferences in the transfer efficiency. Sections III–V are devoted to a detailed analysis of the observed interferences. In Sec. III, a procedure is explained which allows us to predict at which values of the chirp parameter interferences between competing pathways will act constructively or destructively. These predictions are subsequently tested in a numerical model which is introduced in Sec. IV, and which is used in Sec. V to simulate the experiments. Both the increase in the transfer efficiency for down-chirped laser pulses and the occurrence of rotational interferences are reproduced in the calculations.

In recent years a lot of attention has been devoted to the question of how molecular dynamics can be controlled by using tailored laser pulses [11]. A number of schemes have been proposed to control dissociation pathways or isomerization of polyatomic molecules, and a few experimental examples of chirp-controlled electronic excitation of polyatomic molecules have been obtained [12,13]. Stimulated Raman involving rapid adiabatic passage (STIRAP) has also been applied to NO and resulted in significant population of the vibrationally excited states [14,15]. Recently vibrational ladder climbing has been performed in the condensed phase by Heilweil's group [16] and for molecules in the gas phase in our group [17]. Our present study illustrates the importance of taking into account rotational interferences [18] in the analyses of molecular coherent control experiments. Because of the occurrence of rotational interferences optimization of the transfer efficiency in vibrational ladder climbing of the NO molecule relies not only on a correct ordering of the frequencies for successive vibrational transitions (a down chirp instead of an up chirp), but, in addition, on the actual magnitude of the chirp as well.

*Present address: Philips Research Labs, Prof. Holstlaan 4, 5656 AA Eindhoven, The Netherlands.

II. EXPERIMENTAL DATA ON VIBRATIONAL LADDER CLIMBING

In the experiment on vibrational ladder climbing a molecular beam of NO crosses at right angles an infrared laser pulse. The infrared pulse is generated by the free electron laser free-electron laser for infrared experiments (FELIX) [19]. This laser is tunable both in frequency and bandwidth. For the experiments reported here the laser is set at $\nu_c = 1845\,\mathrm{cm}^{-1}$ and $\Delta\nu = 50\,\mathrm{cm}^{-1}$ for a pulse fluence of $\Phi = 25\,\mathrm{mJ\,cm}^{-2}$. The chirp of the laser pulse is controlled with an all reflective shaper operating in the infrared [20]. After exposure to the infrared laser pulse, the rovibrational distribution of the excited NO molecule is probed using the resonantly enhanced multiphoton ionization (REMPI) technique [21,22]. In the experiment (see also [17]) the population of vibrational state $|v\rangle$ is measured by tuning an UV laser with a bandwidth of $\Delta\nu_{\mathrm{UV}} = 1.85\,\mathrm{cm}^{-1}$ to the coinciding $\mathbf{Q}_{11}$ and $\mathbf{P}_{21}$ branches of the NO $A\,^2\Sigma(v') - X\,^2\Pi_{1/2}(v'')$ or NO$(v',v'')\gamma$ bands. Due to the large bandwidth of the UV laser, rotational levels with $J'' \in \{\frac{1}{2},\ldots,4\frac{1}{2}\}$ are probed simultaneously. For the measured rotational temperature of $T_{\mathrm{rot}} = 14\,\mathrm{K}$ almost all population is present in these rotational states. The distribution over the J levels does not shift dramatically after absorption of a few IR photons [17]. Therefore, most of the population in vibrationally excited states is also probed via the same manifold of lines of the low J levels via $\mathbf{Q}_{11}$ and $\mathbf{P}_{21}$ branches of the NO$(v',v'')\gamma$ band. The NO^+ ion signal is amplified by an El-Mul Micro Sphere Plate (MSP). The MSP signal is recorded by a digital oscilloscope and stored in a computer. In a typical experiment the ion yield is recorded for different settings of the pulse shaper and hence for different chirp values.

Figure 1 shows the population in the vibrationally excited states $v=1$ to $v=4$ of NO after exposing the molecules to a chirped infrared laser pulse. The full line represents a model calculation that is discussed in detail in Sec. V. Positive values of α correspond to an increasing laser frequency during the pulse, hence a red-to-blue chirp, while negative values of α correspond to a blue-to-red chirp. The absolute value of α is a measure for the rate at which the frequency changes. A large value of $|\alpha|$ corresponds to a slow change in frequency and therefore a long duration of the pulse. In a molecule like NO where the vibrational transition frequencies decrease for higher excited states, one expects that in a multistep excitation process the transfer is enhanced for negative α.

The top panel in Fig. 1 shows that the population in the first excited state ($v=1$) is independent of the chirp. In the perturbative intensity regime, with little population transfer per vibrational step, the $v=0$ to $v=1$ transition can, to first order, be considered as an isolated two-level system, with initially 99.99% of the population in the ground state. The population in the excited state depends in that case almost exclusively on the power spectrum at the resonant frequency and not on the order of the nonresonant frequencies in the laser pulse. Hence the $v=1$ population is expected to be independent of the chirp.

For two-photon excitation to the $v=2$ state the order of the frequencies is relevant, as can be seen in Fig. 1. For negative chirp the transfer to $v=2$ is enhanced: the molecule is first exposed to the radiation corresponding to the $v=0$ to $v=1$ transition and subsequently to radiation corresponding to the $v=1$ to $v=2$ transition. At positive chirp the population is nonzero despite the frequency order. This population is not due to two-photon excitation from the ground state, but due to the one-photon transfer of thermally present $v=1$ population. Since the thermal population of $v=2$ and $v=3$ is negligible (see Table I), no population is transferred in a one-photon process at positive chirp to $v=3$ and $v=4$, respectively.

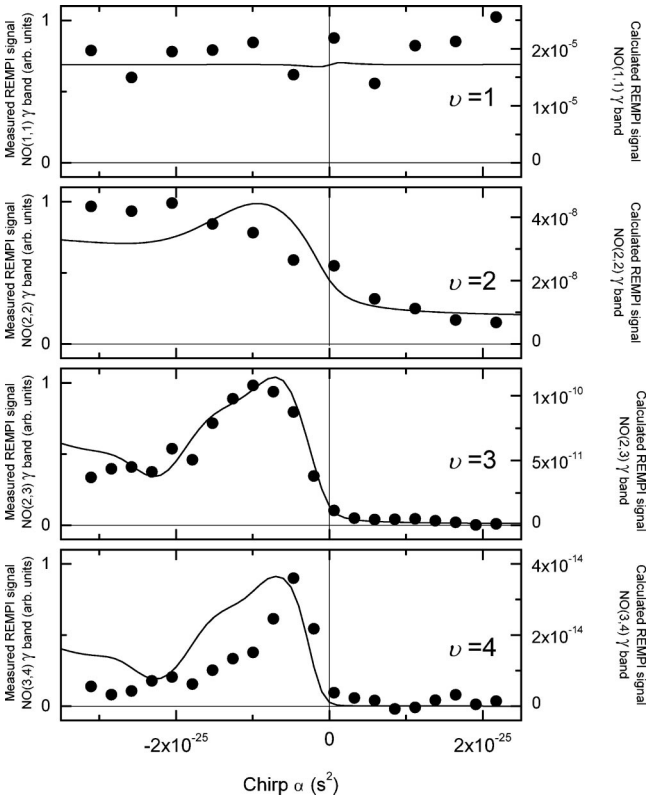

FIG. 1. The measured population of $v''=1$, 2, 3, and 4 as a function of the chirp of the IR laser pulse. The population is probed by 1+1 REMPI via the NO $A\,^2\Sigma(v')$ state. At the band head the low rotational states ($J'' \in \{\frac{1}{2},\ldots,4\frac{1}{2}\}$) of the coinciding $\mathbf{Q}_{11}$ and $\mathbf{P}_{21}$ branches of the NO$(v',v'')\gamma$ bands are probed. The curves are the results of the model calculations discussed in Secs. IV and V.

For the higher vibrational states (i.e., $v=3,4$) we observe an enhanced transfer for negative chirp values as well. Remarkably, the transferred population oscillates as a function of chirp. An intuitive picture of the quantum interference of different rotational excitation routes that causes these oscillations is discussed in the next section.

III. MULTIPLE ROTATIONAL INTERFERENCE IN CLIMBING THE VIBRATIONAL LADDER

A. Interference in three-level ladder systems

We introduce a dressed-state picture of the eigenstates to describe the effect of chirp and contributions of interfering pathways. Figure 2 shows a diagram of the eigenenergies of the dressed states of an anharmonic three-level system as a function of the photon energy. The ground state $|0\rangle$ is dressed (pushed up) by 1 photon and has an eigenfrequency of $\nu_0 + \nu$, where ν is the laser frequency and ν_0 the undressed

TABLE I. The thermal initial population distribution over the rovibrational states $|v,J\rangle$ (with $v \in \{0,...,4\}$ and $J \in \{\frac{1}{2},...,8\frac{1}{2}\}$) for $T_{\rm rot} = 14$ K and $T_{\rm vib} = 300$ K, i.e., temperature case (II) of the calculation. Each sublevel $|v,J,m_J\rangle$ is populated by $P_{m_J} = P_J/(2J+1)$, with P_J the $|v,J\rangle$ population, corresponding to an isotropic initial distribution. Numbers in square brackets indicate powers of ten.

$v\backslash J$	$\frac{1}{2}$	$1\frac{1}{2}$	$2\frac{1}{2}$	$3\frac{1}{2}$	$4\frac{1}{2}$	$5\frac{1}{2}$	$6\frac{1}{2}$	$7\frac{1}{2}$	$8\frac{1}{2}$
0	0.298	0.356	0.226	0.906[−1]	0.241[−1]	0.437[−2]	0.547[−3]	0.474[−4]	0.287[−5]
1	0.369[−4]	0.440[−4]	0.280[−4]	0.112[−4]	0.298[−5]	0.541[−6]	0.676[−7]	0.587[−8]	0.356[−9]
2	0.522[−8]	0.624[−8]	0.396[−8]	0.158[−8]	0.423[−9]	0.766[−10]	0.957[−11]	0.831[−12]	0.503[−13]
3	0.845[−12]	0.101[−11]	0.642[−12]	0.257[−12]	0.684[−13]	0.124[−13]	0.155[−14]	0.135[−15]	0.815[−17]
4	0.156[−15]	0.187[−15]	0.119[−15]	0.476[−16]	0.127[−16]	0.230[−17]	0.287[−18]	0.249[−19]	0.151[−20]

eigenfrequency of the wave function. The intermediate state $|1\rangle$ is undressed and its eigenfrequency (ν_1) is independent of the laser frequency. The top state $|2\rangle$ is dressed (pulled down) by -1 photon, and has an eigenfrequency of $\nu_2 - \nu$ in the laser field. The dressed ground state crosses the intermediate $v=1$ state at the frequency ν_{10} and a similar crossing occurs between the intermediate state and the final state. At ν_{21} the dressed ground state ($\nu_0 + \nu$) and the dressed final state ($\nu_2 - \nu$) intersect and a direct two-photon transition is possible. The ladder anharmonicity δ is defined as $[\nu_{21} - \nu_{10}]$. For vibrational ladders $\delta_{\rm vib} \approx -2 \times \omega_e x_e$ (see [23], with for NO $\omega_e x_e = 14.187\ {\rm cm}^{-1}$.) The dressed-level scheme as shown in Fig. 2 is drawn for a ladder system with a negative anharmonicity $\delta < 0$, which is a general feature of vibrational ladders in molecules such as NO. At the end of Sec. III C, when the rotational structure of a molecule is included, the sign of the anharmonicity of the rovibrational ladder is shown to be a function of the rotational quantum number J.

With the help of Fig. 2 we can describe the general features of the interaction of a chirped laser pulse with a three-level system. For a chirped laser pulse, the instantaneous photon frequency is a function of time [see Eq. (A1)]. The begin and end times are determined by the upper and lower limits of the spectral energy in the laser bandwidth and the relationship between time, chirp, and the instantaneous frequency. Suppose that the laser pulse has a negative chirp and we start in the ground state (top right in Fig. 2). While the radiation frequency is decreasing we encounter the transition to the first excited state at ν_{10} and the population can be transferred to this state (adiabatic passage). Now we are at the intermediate state (horizontal line) and encounter the second transition frequency at ν_{21} where the population can be transferred to the final state $|2\rangle$. This population transfer process, with the intuitive frequency order, is marked as path I in the figure. An alternative route to populate the top state starting from the ground state is shown as path II. In this route the population is not transferred at the subsequent resonance frequencies (which are traversed diabatically), but direct at the two-photon resonance frequency. Each of the two paths accumulates its own phase. The phase difference is determined by the time interval between the crossing of resonances and on the magnitude of the anharmonicity of the ladder. Since the above-mentioned time interval depends on the speed of the frequency sweep (i.e., on the chirp), the accumulated phase difference between the paths is a function of the chirp. For sufficiently large chirp the instantaneous frequency of a Gaussian laser pulse increases linearly in time. Under this condition the phase difference is proportional to the chirp, and the oscillation period $\alpha_{2\pi}$ can be defined as the length of the interval between two subsequent chirp values for which the phase difference equals 2π.

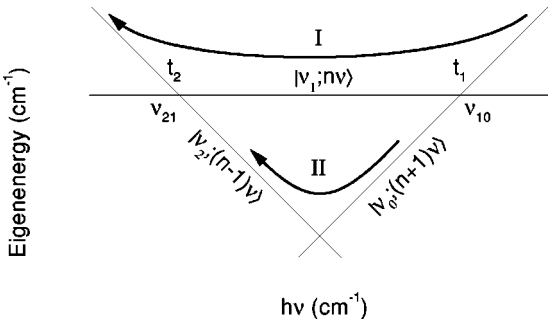

FIG. 2. A dressed-level energy diagram of the eigenenergies of a three-level system. The lines show the unperturbed dressed-state eigenenergies as a function of laser-field frequency (ν). The levels are labeled $|\nu_0;(n+1)\nu\rangle$, $|\nu_1;n\nu\rangle$, and $|\nu_2;(n-1)\nu\rangle$. The transition frequencies are indicated by ν_{10} and ν_{21}. For a Gaussian laser pulse with chirp α, the frequency axis becomes a time axis as well, with, for large α, $t = 4\pi\alpha(\nu - \nu_c)$. In the limit of weak coupling of the states, the traversion times t_1 and t_2 of the level crossings can be calculated from the transition frequencies $\nu_{10} = \nu_1 - \nu_0$ and $\nu_{21} = \nu_2 - \nu_1$. The relationship between accumulated phase difference and the area enclosed by the two routes is discussed in the Appendix.

In the paper of Balling *et al.* [9] both the experimental results and the model calculations on the three-level rubidium ladder system (i.e., the electronic ladder formed by the $5s$-$5p$-$5d$ states) showed an oscillatory behavior in the $|{\rm top}\rangle$ state population as a function of the chirp of the laser pulse. These oscillations were attributed to quantum interference [24] between two excitation paths, both contributing to the final top-state population.

Now we derive a relation between the area enclosed by two pathways (e.g., I and II as shown in Fig. 2) and the oscillation period $\alpha_{2\pi}$ of the interference. The period of the interference wiggles can be explained by phase differences between the interfering paths. The two paths correspond to different dressed-state energies $\hbar W$. Since the wave function contains a factor $\exp(iWt)$, the phases of the wave functions that follow the different paths evolve differently. Both paths contribute to the population transfer from the ground state $|0\rangle$ to the final state $|2\rangle$. The magnitude of the phase difference depends on the energy difference between the paths and the time it takes to chirp from the first to the second resonance. The time interval is determined by the chirp α of the laser pulse in combination with the frequency difference δ be-

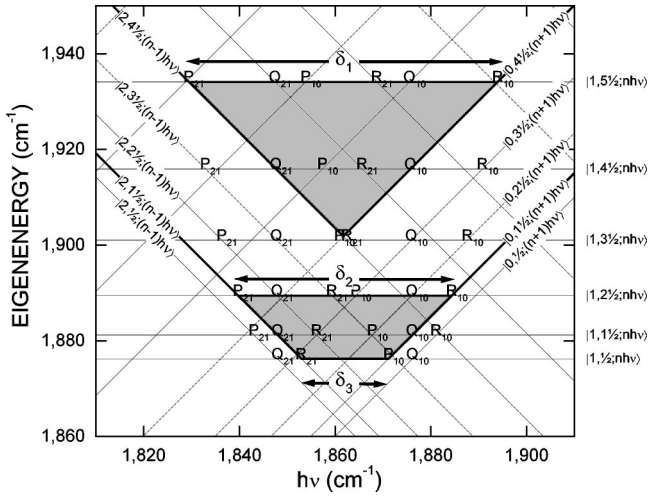

FIG. 3. A dressed-level energy diagram of the eigenenergies of the rotational manifold for three lowest vibrational states of the NO molecule. The lines show the unperturbed energies as a function of laser-field frequency ($h\nu$). Parallel lines belong to different rotational levels J of the same vibrational state $|v\rangle$ and are labeled $|v,J;nh\nu\rangle$. The boldface symbols represent the dipole-allowed couplings by $\mathbf{P}_{v'v''}$-, $\mathbf{Q}_{v'v''}$-, and $\mathbf{R}_{v'v''}$-type transitions. The two basic interference paths are indicated. The triangle represents interference $Q_{2\mathrm{ph}}-Q_{PR}(4\frac{1}{2})$, i.e., between the two-photon path and the path with the two resonant transitions $\mathbf{P}_{21}(5\frac{1}{2})\leftarrow\mathbf{R}_{10}(4\frac{1}{2})$. One can calculate the interference frequency $\alpha_{2\pi}=\pi/A$ from the enclosed area $A_{\mathrm{tri}}=(\delta_1/2)^2$, with $\delta_1=-64.55\,\mathrm{cm}^{-1}$ the anharmonicity between these transitions. The trapezium shows the interference paths $Q_{PR}-Q_{RP}(1\frac{1}{2})$, with $A_{\mathrm{tra}}=[(\delta_2/2)^2-(\delta_3/2)^2]$ and $\delta_2=-44.66\,\mathrm{cm}^{-1}$, $\delta_3=-18.22\,\mathrm{cm}^{-1}$.

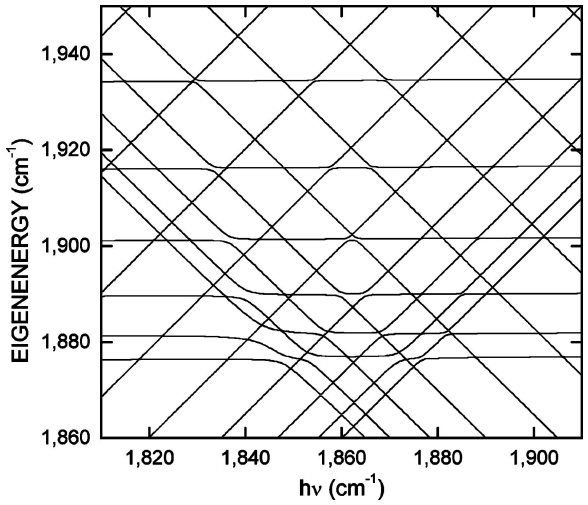

FIG. 4. A dressed-level energy diagram of the eigenenergies of sublevel $m_J=0$ of the rotational manifold for three lowest vibrational states of the NO molecule interacting with a chirped laser pulse ($\alpha=2.0\times10^{-25}\,\mathrm{s}^2$). All model-pulse parameters equal the experimental pulse, except for an increase of the fluence: $\Phi_{\mathrm{calc}}=100\times\Phi_{\mathrm{expt}}$, to increase the visibility of the level splittings induced by the molecule–laser-field interaction.

tween the transitions. The phase difference is a linear function of the chirp, and sinusoidal oscillations in the transfer to the top level (as a function of the chirp) are observed. For the enclosed area between two pathways in the dressed-level diagram of a magnitude A, the interference period $\alpha_{2\pi}$ is given as (see the Appendix)

$$\alpha_{2\pi}=\frac{\pi}{A}. \tag{1}$$

Equation (1) may be used as long as the instantaneous frequency increases linearly in time, which is the case for a strongly chirped laser pulse (i.e., having a pulse duration that is at least three times larger than the transform limited pulse) with a Gaussian temporal profile.

B. Introduction of a nomenclature for the excitation paths in a rovibrational ladder system

The vibrational ladder system in NO is more complicated than the simple three-level system treated in the preceding section. First, a large number of vibrational states ($v_{\max}=37$) is present in the potential well of the electronic ground state $X\,^2\Pi_{1/2}$ [23]. In addition, each vibrational state is split into a number of rotational states. Figure 3 displays a zero-laser-field-strength dressed-level energy diagram of the eigenenergies $|0,J'';(n+1)h\nu\rangle$, $|1,J';nh\nu\rangle$, and $|2,J;(n-1)h\nu\rangle$ of the three lowest vibrational states of the NO molecule as a function of the photon energy ($h\nu$). Parallel lines represent different rotational states belonging to the same vibrational level. The positions of the dipole-allowed **P**, **Q**, and **R** transitions from vibrational level v'' to v' are indicated by the symbols $\mathbf{P}_{v'v''}$, $\mathbf{Q}_{v'v''}$, and $\mathbf{R}_{v'v''}$. When the dipole coupling between the dressed rovibrational levels is included in the Hamiltonian, the degeneracies of the dressed states at the positions indicated by these symbols are removed for non-zero-laser-field strengths. This situation for states with $m_J=0$ (i.e., when all rotational states are allowed to couple) is depicted in Fig. 4 for a laser intensity of $I=8.5\times10^{11}\,\mathrm{W\,cm}^{-2}$, which corresponds to an electric-field strength of $F=2.6\times10^9\,\mathrm{V\,m}^{-1}$, as calculated for a pulse with chirp $\alpha=2\times10^{-25}\,\mathrm{s}^2$ and $\tau(\alpha)=3.0\,\mathrm{ps}$ (with shortest duration $\tau_0=379\,\mathrm{fs}$ at $\alpha=0\,\mathrm{s}^2$). Depending on the strength of the dipole coupling (determined by the IR intensity) and the rate of frequency sweep (determined by the chirp) the avoided crossings of the dressed states are traversed either more or less adiabatically. There is a large number of interfering paths that start from a specific rotational level J'' in the vibrational ground state $|0,J''\rangle$ and lead to population transfer to excited state $|2,J\rangle$. For the definition of a specific path the following nomenclature is introduced: a total difference in rotational quantum number $\Delta J=(J-J'')$ between initial and final state is called a $\Delta J_{YX}(J)$ path, where $\Delta J\in\{O,P,Q,R,S\}$ and $X,Y\in\{P,Q,R,2\mathrm{ph}\}$, corresponding to a series of resonant dipole-allowed $\mathbf{P}_{v'v''}$, $\mathbf{Q}_{v'v''}$, or $\mathbf{R}_{v'v''}$ transitions, or to a direct two-photon process. For $\Delta J=-2$, -1, 0, 1 or 2, the path symbol is O_{YX}, P_{YX}, Q_{YX}, R_{YX}, or S_{YX}, respectively, after the general convention used in [23,25]. To discriminate transitions towards lower vibrational states, the symbols $\overline{X}$ or $\overline{Y}$ are used (e.g., pathway Q_{PR} leaves a molecule in the same state as it started: $|v,J\rangle\rightarrow|v+1,J+1\rangle\rightarrow|v,J\rangle$). The subscripts X,Y identify the consecutive sequence of transitions, describing each path in a unique way. For example, the gray triangle in Fig. 3 is enclosed by two paths that transfer population from $|v'',J''\rangle=|0,4\frac{1}{2}\rangle$ to

TABLE II. The label, the consecutive transitions, and the intermediate states for all possible paths for two-photon processes that populate $|2,J\rangle$ from $|0,J''\rangle$.

		O paths	
O_{PP}	$=\mathbf{P}_{21}\mathbf{P}_{10}$	$\equiv\|2,J;(n-1)h\nu\rangle$	$\leftarrow\|1,J+1;nh\nu\rangle \leftarrow\|0,J+2;(n+1)h\nu\rangle$
O_{2ph}	$=\mathbf{O}_{20}$	$\equiv\|2,J;(n-1)h\nu\rangle$	$\leftarrow\|\text{virtual state}\rangle \leftarrow\|0,J+2;(n+1)h\nu\rangle$
		P paths	
P_{QP}	$=\mathbf{Q}_{21}\mathbf{P}_{10}$	$\equiv\|2,J;(n-1)h\nu\rangle$	$\leftarrow\|1,J;nh\nu\rangle \leftarrow\|0,J+1;(n+1)h\nu\rangle$
P_{PQ}	$=\mathbf{P}_{21}\mathbf{Q}_{10}$	$\equiv\|2,J;(n-1)h\nu\rangle$	$\leftarrow\|1,J+1;nh\nu\rangle \leftarrow\|0,J+1;(n+1)h\nu\rangle$
P_{2ph}	$=\mathbf{P}_{20}$	$\equiv\|2,J;(n-1)h\nu\rangle$	$\leftarrow\|\text{virtual state}\rangle \leftarrow\|0,J+1;(n+1)h\nu\rangle$
		Q paths	
Q_{PR}	$=\mathbf{P}_{21}\mathbf{R}_{10}$	$\equiv\|2,J;(n-1)h\nu\rangle$	$\leftarrow\|1,J+1;nh\nu\rangle \leftarrow\|0,J;(n+1)h\nu\rangle$
Q_{RP}	$=\mathbf{R}_{21}\mathbf{P}_{10}$	$\equiv\|2,J;(n-1)h\nu\rangle$	$\leftarrow\|1,J-1;nh\nu\rangle \leftarrow\|0,J;(n+1)h\nu\rangle$
Q_{QQ}	$=\mathbf{Q}_{21}\mathbf{Q}_{22}$	$\equiv\|2,J;(n-1)h\nu\rangle$	$\leftarrow\|1,J;nh\nu\rangle \leftarrow\|0,J;(n+1)h\nu\rangle$
Q_{2ph}	$=\mathbf{Q}_{20}$	$\equiv\|2,J;(n-1)h\nu\rangle$	$\leftarrow\|\text{virtual state}\rangle \leftarrow\|0,J;(n+1)h\nu\rangle$
		R paths	
R_{QR}	$=\mathbf{Q}_{21}\mathbf{R}_{10}$	$\equiv\|2,J;(n-1)h\nu\rangle$	$\leftarrow\|1,J;nh\nu\rangle \leftarrow\|0,J-1;(n+1)h\nu\rangle$
R_{RQ}	$=\mathbf{R}_{21}\mathbf{Q}_{10}$	$\equiv\|2,J;(n-1)h\nu\rangle$	$\leftarrow\|1,J-1;nh\nu\rangle \leftarrow\|0,J-1;(n+1)h\nu\rangle$
R_{2ph}	$=\mathbf{R}_{20}$	$\equiv\|2,J;(n-1)h\nu\rangle$	$\leftarrow\|\text{virtual state}\rangle \leftarrow\|0,J-1;(n+1)h\nu\rangle$
		S paths	
S_{RR}	$=\mathbf{R}_{21}\mathbf{R}_{10}$	$\equiv\|2,J;(n-1)h\nu\rangle$	$\leftarrow\|1,J-1;nh\nu\rangle \leftarrow\|0,J-2;(n+1)h\nu\rangle$
S_{2ph}	$=\mathbf{S}_{20}$	$\equiv\|2,J;(n-1)h\nu\rangle$	$\leftarrow\|\text{virtual state}\rangle \leftarrow\|0,J-2;(n+1)h\nu\rangle$

$|2,4\frac{1}{2}\rangle$ either via $|1,5\frac{1}{2}\rangle$, labeled $Q_{PR}(4\frac{1}{2})$, or via a two-photon transition, labeled $Q_{2\text{ph}}(4\frac{1}{2})$. Both paths contribute to the population of $|2,4\frac{1}{2}\rangle$. To gain some insight into which paths can occur, in Table II the label, the consecutive transitions, and the intermediate states for all possible paths that populate $|2,J\rangle$ from $|0,J''\rangle$ are displayed.

The above-introduced labeling system can easily be extended for higher-order photon processes by extending the number of subscripts. For example, populating $|3,4\frac{1}{2}\rangle$ from $|0,1\frac{1}{2}\rangle$ by the three consecutive single-photon transitions $\mathbf{R}_{32}(3\frac{1}{2})$, $\mathbf{R}_{21}(2\frac{1}{2})$, $\mathbf{R}_{10}(1\frac{1}{2})$ is labeled by $T_{RRR}(4\frac{1}{2})$.

C. Strength of interfering pathways

Returning to the gray triangle of Fig. 3, its enclosed area can be attributed uniquely to interference between $Q_{PR}(4\frac{1}{2})$ and $Q_{2\text{ph}}(4\frac{1}{2})$. The corresponding oscillation period can be calculated from Eq. (1) with $\delta_1(4\frac{1}{2})=\{\nu[\mathbf{P}_{21}(5\frac{1}{2})]-\nu[\mathbf{R}_s(4\frac{1}{2})]\}=-64.55\,\text{cm}^{-1}$ to be $\alpha_{2\pi}^{Q_{PR}-Q_{2\text{ph}}}(4\frac{1}{2})=8.486\times10^{-26}\,\text{s}^2$. The gray trapezium in Fig. 3 shows the area enclosed by paths $Q_{PR}(1\frac{1}{2})$ and $Q_{RP}(1\frac{1}{2})$. Its area is $A_{\text{tra}}=[(\delta_2/2)^2-(\delta_3/2)^2]$ with $\delta_2(1\frac{1}{2})=\{\nu[\mathbf{P}_{21}(2\frac{1}{2})]-\nu[\mathbf{R}_{10}(1\frac{1}{2})]\}=-44.66\ \text{cm}^{-1}$ and $\delta_3(1\frac{1}{2})=\{\nu[\mathbf{R}_{21}(\frac{1}{2})]-\nu[\mathbf{P}_{10}(1\frac{1}{2})]\}=-18.22\ \text{cm}^{-1}$, corresponding to a period of $\alpha_{2\pi}^{Q_{PR}-Q_{RP}}(1\frac{1}{2})=2.123\times10^{-25}\,\text{s}^2$.

There are two conditions determining the contribution of each path to the population transfer to the upper state. First, its contribution is proportional to the product of the Rabi frequency of the two transitions. In general, paths containing **Q** transitions only play a role for the lowest rotational states, since their Hönl-London factors are small compared to those for **P** and **R** transitions ($F_{\text{HL}(Q)}<0.01$ for $J\geqslant4\frac{1}{2}$) [26]. Secondly, to enhance the transfer for a given sign of the chirp of the laser pulse, the instantaneous frequency has to follow the ordering of transition frequencies. Whether this condition is met depends on the sign of the chirp, the rotational quantum number J, and on the spectroscopic parameters for the vibrational frequency ω_e, the anharmonic constant $\omega_e x_e$, and the rotational constant B_e of the particular molecule (see, e.g., [23]). Since the direct two-photon excitation occurs at a single frequency, the $Y_{2\text{ph}}$ paths always meet this condition. The paths P_{PQ}, Q_{PR}, Q_{QQ}, and R_{QR} clearly have a negative anharmonicity for all J levels, and contribute for $\alpha<0$ only. However, for the other paths (P_{QP}, Q_{RP}, and R_{RQ}) the condition sets restrictions on the subset of J values for which population transfer is allowed. This subset is different for both signs of the chirp. For example, transfer to the $v''=2$ state of the NO molecule with the chirp $\alpha<0$, the path $P_{QP}(J)$ is allowed for $J\in\{1\frac{1}{2},\ldots,6\frac{1}{2}\}$ only. For the reverse sign of the chirp, this path is allowed for $J\geqslant7\frac{1}{2}$. Similarly, for $\alpha<0$ the path $Q_{RP}(J)$ is allowed for $J\in\{1\frac{1}{2},2\frac{1}{2},3\frac{1}{2}\}$ and for $\alpha>0$ for $J\geqslant4\frac{1}{2}$. Finally, for $\alpha<0$ the path $R_{RQ}(J)$ is allowed for $J\in\{1\frac{1}{2},\ldots,8\frac{1}{2}\}$ and for $J\geqslant9\frac{1}{2}$ if $\alpha>0$.

The anharmonicity corresponding to a specific path of the rovibrational ladder is the sum of the anharmonicities of the rotational and vibrational ladder: $\delta_{\text{rovib}}(J)=\delta_{\text{rot}}(J)+\delta_{\text{vib}}$. The sign of δ_{rovib} is a function of the rotational quantum number J. This can be attributed to the competition between the positive anharmonicity of the rotational ladder [$\delta_{\text{rot}}(J)\sim J$] and the negative anharmonicity of the vibrational ladder. Obviously, when multiple consecutive transitions to higher vibrational levels are involved, the anharmonicity can change sign, which would frustrate population transfer along such a path by a laser pulse with a linear chirp. This topic is discussed in more detail in Sec. V C.

IV. DRESSED-STATE DESCRIPTION OF COHERENT CONTROL OF MOLECULAR VIBRATIONAL EXCITATION

In this section we describe the formalism for calculating the time evolution of the molecular wave function in the vibrational excitation scheme. As a result of the chirped laser excitation, a coherent superposition of rovibrational states is formed. This situation is conveniently described using the dressed-molecule approach, where the propagation of the superposition is calculated in a frame which rotates at the instantaneous optical frequency of the excitation laser. In this approach, the superposition is decomposed in eigenstates of the molecule plus field Hamiltonian. The expansion coefficients of the molecular wave function in terms of these states are stationary as long as the laser field is constant, and only change with the amplitude or frequency of the laser field, which are slowly varying functions of time. The molecular vibrational excitation can be analyzed in terms of an adiabatic or diabatic propagation over curves corresponding to individual dressed eigenstates (depending on the behavior at the series of avoided crossings which are encountered).

The time dependence of the molecular wave function is given by the Schrödinger equation as

$$i\hbar \frac{d\Psi(t)}{dt} = H(t)\Psi(t) = [H_0 + \vec{\mu}\cdot\vec{F}(t)]\Psi(t). \tag{2}$$

Here H_0 represents the molecular Hamiltonian and $\vec{\mu}\cdot\vec{F}(t)$ represents the interaction of the molecule, with dipole moment $\vec{\mu}$ with the (chirped) laser field $\vec{F}(t)$. The wave function can be expanded in terms of the rotational and vibrational eigenfunctions of the electronic ground state $X\ ^2\Pi_{1/2}$ according to

$$\Psi(t) = \sum_{v=0}^{v_{\max}} \sum_{J=0}^{\infty} a_{v,J}(t)\psi_{v,J}. \tag{3}$$

The laser field $\vec{F}(t)$ couples rotational levels of one vibrational state $X\ ^2\Pi_{1/2}(v'')$ with levels in the adjacent vibrational states $X\ ^2\Pi_{1/2}(v')$, where $|v''-v'|=1$. All vibrational states are $^2\Pi$ states, hence the couplings are subject to the selection rule $\Delta J = 0, \pm 1$, where the relative coupling strength is calculated from the Hönl-London factors (F_{HL}) for $^2\Pi$-$^2\Pi$ transitions [26] and the appropriate $3J$ symbols [27]. The electric field of the laser pulse is linearly polarized in the z direction and taken Gaussian in the time domain:

$$\vec{F}(t) = F_{\max}\vec{e}_z \tfrac{1}{2}\{\exp[-\Gamma(\alpha)t^2]\exp(i\omega_c t) + \text{c.c.}\}, \tag{4}$$

where $\Gamma(\alpha)$ is given by

$$\Gamma(\alpha) = \left(\frac{8\ln 2}{\Delta\omega^2} + 4i\alpha\right)^{-1}, \tag{5}$$

with $\Delta\omega$ the bandwidth of the short laser pulse of central frequency $\omega_c = 2\pi\nu_c$ and α the amount of chirp.

Substitution of the expansion of the wave function Eq. (3) into the time-dependent Schrödinger equation, Eq. (2), left multiplying by $\psi^*_{v,J}$, and integration over space yields the following equation for the time dependence of the expansion coefficients $a_{v,J}(t)$:

$$i\hbar\dot{a}_{v,J}(t) = E_{v,J}a_{v,J}(t) + \sum_{v'}\sum_{J'=J-1}^{J'=J+1} a_{v',J'}(t)\langle\psi_{v,J}|\vec{\mu}\cdot\vec{F}(t)|\psi_{v',J'}\rangle, \tag{6}$$

where $E_{v,J}$ is the eigenenergy of state $|v',J'\rangle$. Next, the propagation of the wave packet is transferred to a rotating frame, by writing the expansion coefficients as

$$a_{v,J}(t) = \sum_{n=-\infty}^{\infty} \underline{a}_{v,J,n}(t)e^{in\omega_c t}, \tag{7}$$

where the coefficients $\underline{a}_{v,J,n}(t)$ now are slowly varying functions of time. Substitution into Eq. (6), requiring that for each n the individual orders of $e^{in\omega_c t}$ are equal on both sides of Eq. (6) yields

$$\begin{aligned} i\hbar\dot{\underline{a}}_{v,J,n}(t) = {} & (E_{v,J} + \hbar n\omega_c)a_{v,J,n}(t) \\ & + \sum_{J'=J-1}^{J'=J+1} a_{v+1,J'n-1}(t)\langle\psi_{v,J}|\vec{\mu}\cdot\vec{\tilde{F}}(t)|\psi_{v+1,J'}\rangle \\ & + \sum_{J'=J-1}^{J'=J+1} a_{v-1,J',n+1}(t)\langle\psi_{v,J}|\vec{\mu}\cdot\vec{\tilde{F}}^*(t)|\psi_{v-1,J'}\rangle, \end{aligned} \tag{8}$$

with

$$\vec{\tilde{F}}(t) = F_{\max}\vec{e}_z \tfrac{1}{2}\exp(-\Gamma t^2). \tag{9}$$

Compared to Eq. (6) the eigenenergy $E_{v,J}$ has been replaced by a dressed-state energy $E_{v,J}+\hbar n\omega_c$, which can be interpreted as the total energy of the molecule and the laser field. According to Eq. (8) different molecular and photon-number states are coupled by single-photon laser transitions. In principle, Eq. (8) describes an infinite series of coupled differential equations. However, in the rotating wave approximation (RWA), where far off-resonant couplings from $|v,J;n\nu\rangle$ to $v',J';\hbar n'\nu\rangle$ are neglected, the mathematical treatment can be considerably simplified. In the RWA the infinite ladder of interacting dressed states is separated into finite blocks of self-contained states which only interact among themselves. The rotational-state-dependent transition matrix elements in Eq. (8) are replaced by the representative single-photon transition matrix elements $\Omega^{v',J',m'_J}_{v,J,m_J}(t)$. With these simplifications, Eq. (8) reduces to

$$\begin{aligned} i\hbar\dot{\underline{v}}_{v,J,n}(t) = {} & (E_{v,J} + \hbar n\omega_c)\underline{a}_{v,J,n}(t) \\ & + \sum_{J'=J-1}^{J'=J+1} \underline{a}_{v+1,J',n-1}(t)\Omega^{v+1,J',m'_J}_{v,J,m_J}(t) \\ & + \sum_{J'=J-1}^{J'=J+1} \underline{a}_{v-1,J',n+1}(t)[\Omega^{v-1,J',m'_J}_{v,J,m_J}(t)]^*, \end{aligned} \tag{10}$$

where $\Omega_{v,J,m_J}^{v',J',m_J'}(t)$ is the Rabi frequency for single-photon excitation:

$$\Omega_{v,J,m_J}^{v',J',m_J'}(t)=\frac{2\vec{\mu}_{v,v'}\cdot\vec{F}(t)}{\hbar}\times F_{\mathrm{HL}}(v,J,v',J')\times\begin{pmatrix} J' & 1 & J \\ m_J' & 0 & -m_J \end{pmatrix}^2. \tag{11}$$

The coupled Eqs. (8) for the coefficients $a_{v,J,n}(t)$ can be written in matrix form as

$$\dot{a}_i(t)=\sum_j H_{ij}(t)a_j(t). \tag{12}$$

The ability to control the efficiency of molecular vibrational excitation using chirped laser pulses enters through the presence of the chirp α in $\Gamma(\alpha)$ in the dressed-state Hamiltonian. Equation (12) can be solved using standard numerical techniques.

In the present problem the laser field couples molecular eigenstates subject to the selection rules $\Delta J=0,\pm 1$, $\Delta m_J=0$. For each initially populated state with total rotational angular momentum J, the projection of the angular momentum m_J is restricted to $|m_J|\in\{\frac{1}{2},\ldots,J\}$. For given laser-field conditions the dressed-state Hamiltonian describes the couplings among *all* levels for a given m_J.

The final population distribution after the excitation by the chirped laser pulse is computed by integrating the time-dependent Schrödinger equation over the pulse duration, where, if the variations in the laser field $\tilde{F}$ are rather slow [Eq. (9)], large time steps for the numerical integration are allowed. Since the ac-Stark shift [28] of the eigenstates is described by the mixing of the unperturbed eigenstates, a larger number of states must be used as basis set. In order to obtain converged results, typically 5–10 rotational states were included for each of the 3–7 vibrational levels of the NO $X\ ^2\Pi_{1/2}$ electronic ground state that were included. The calculation predicts how the probability amplitude of every single state $|v,J,m_J\rangle$ is redistributed over all other $|v,J,m_J\rangle$ states. To obtain the final-state population distribution over the $|v,J,m_J\rangle$ states, the incoherent sum is calculated by multiplying the computed redistribution matrix with the vector that describes the initial population distribution over the states $|v,J,m_J\rangle$.

V. RESULTS OF CALCULATIONS

A. Most relevant interference pathways

In this subsection the appearance and origin of the rotational interferences is more closely examined. We first present results of calculations using a relatively small basis set, which allows us to perform the calculations over a significantly wider range of chirp than a fully converged calculation. Using the model described in the preceding section, calculations were performed for the vibrational excitation of the electronic ground state $X\ ^2\Pi_{1/2}$ of the NO molecule by a chirped IR ($h\nu=1850\,\mathrm{cm}^{-1}$, $\Delta h\nu=50\,\mathrm{cm}^{-1}$) laser pulse that is Gaussian in the time domain with a fluence $\Phi=25\,\mathrm{mJ\,cm}^{-2}$. For $\alpha=0$, the pulse duration is $\tau_0=0.4$ ps. At the corresponding peak intensity ($I_{\max}=83\times10^9\,\mathrm{W\,cm}^{-2}$) the single-photon Rabi frequencies are typically less than $\Omega_{v,J,m_J}^{v',J',m_J'}\leq 1\times10^{11}\,\mathrm{rad\,s}^{-1}$, with $m_J'=m_J$ since the laser field is linearly polarized. The values of the set of parameters used in the simulation correspond to the conditions of the experiment.

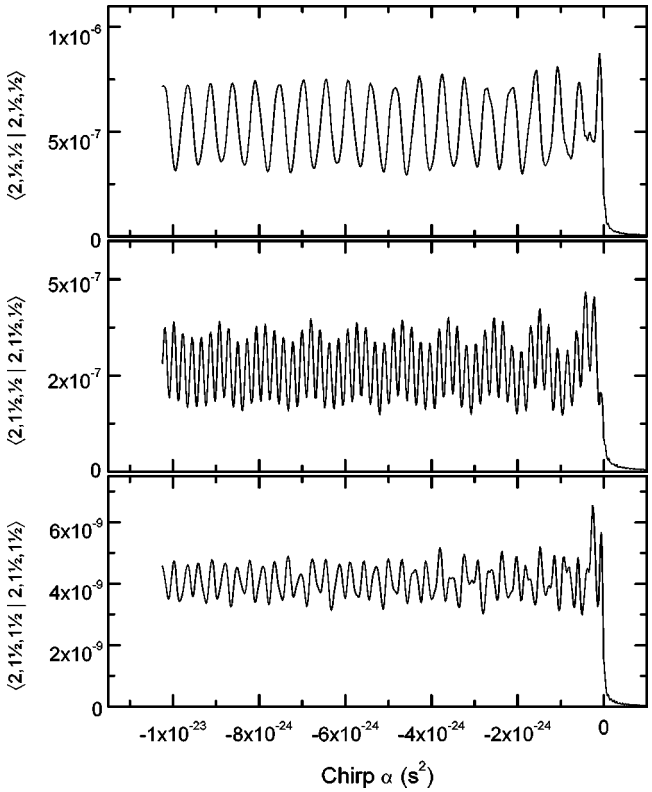

FIG. 5. The top panel shows the population in $|v,J,m_J\rangle=|2,\frac{1}{2},\frac{1}{2}\rangle$ as a function of the chirp α, as calculated for an IR laster pulse with $h\nu=1850\,\mathrm{cm}^{-1}$, $\Delta h\nu=50\,\mathrm{cm}^{-1}$, and a fluence of $\Phi=25\,\mathrm{mJ\,cm}^{-2}$. The presence of multiple interferences is obvious. The middle and bottom panel display the population of $|2,1\frac{1}{2},\frac{1}{2}\rangle$ and $|2,1\frac{1}{2},1\frac{1}{2}\rangle$, respectively. Note the remarkable difference in the behavior of the two different m_J sublevels in the same rotational states J. The initial state was a Boltzmann distribution over four rotational levels ($J''\in\{\frac{1}{2},\ldots,3\frac{1}{2}\}$) with all their m_J'' sublevels of three vibrational states ($v''\in\{0,1,2\}$) with $T_{\mathrm{rot}}=14$ K and $T_{\mathrm{vib}}=1$ K.

Figure 5 shows the predicted population distribution, as calculated using four rotational levels $J''\in\{\frac{1}{2},\ldots,3\frac{1}{2}\}$, and the corresponding sublevels m_J, for each of the three vibrational states $v''\in\{0,1,2\}$, as a function of the chirp α in the excited vibrational state $|2,J,m_J\rangle$ (from top to bottom panel, respectively, $|2,\frac{1}{2},\frac{1}{2}\rangle$, $|2,1\frac{1}{2},\frac{1}{2}\rangle$, and $|2,1\frac{1}{2},1\frac{1}{2}\rangle$). At first inspection it is clear from the irregular oscillatory behavior that multiple interference periods are present. This is in contrast with the sinusoidal behavior of the oscillations as a function of the chirp in the simple three-level ladder system in rubidium [9,10].

For each of the individual $|J,m_J\rangle$ levels of the $v''=2$ state the population oscillates with a different set of periods. To identify the contributions of the different interfering pathways the results shown in Fig. 5 are Fourier transformed

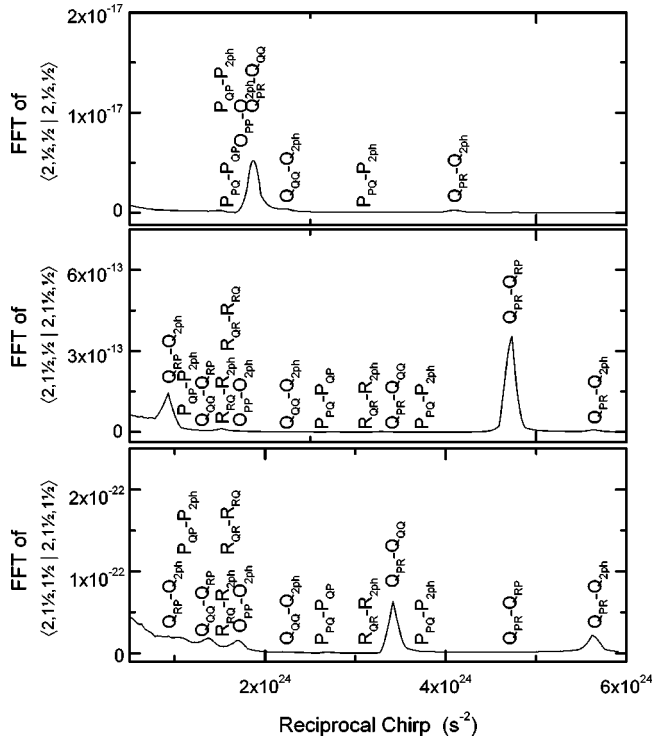

FIG. 6. The three panels display Fourier transforms of the population of, respectively, $|2,\frac{1}{2},\frac{1}{2}\rangle$, $|2,1\frac{1}{2},\frac{1}{2}\rangle$, and $|2,1\frac{1}{2},1\frac{1}{2}\rangle$, as they are shown in Fig. 5. The labels indicate the predicted interference frequencies as calculated from the enclosed areas (see Sec. III and Appendix).

after multiplication with a Hanning window [29]. The calculation was performed for a large number ($N=2^9$) of equidistant chirp values, providing a sufficient spectral resolution in a fast Fourier transform (FFT) to identify interference periods with pairs of interfering paths. Figure 6 shows the FFT of the population transferred to each of the $|2,J,m_J\rangle$ levels. The labels in Fig. 6 indicate the frequencies $\alpha_{2\pi}$ (see also Table III) as calculated from the different enclosed areas [using Eq. (1)], corresponding to the pairs of interfering paths. Obviously, each peak corresponds to a pair of interfering pathways. However, there is not always a peak present with every label. In the low intensity regime the peak height is proportional to the product of the Rabi frequencies [see Eq. (11)] of the two interfering paths. For certain transitions the Hönl-London factors are small, resulting in relatively small Rabi frequencies for those particular transitions.

Summarizing, the period of the interference in population as a function of the chirp can be identified with the enclosed areas between the interfering pathways and the most important contribution comes from the two paths with the largest product of their Rabi frequencies.

B. Interference in the population as a function of chirp

Next, the model discussed in Sec. IV was applied to simulate the experiments discussed in Sec. II. Calculations were performed with laser-pulse parameters that equal those for experiments performed at FELIX [17]. The population redistribution over the rovibrational states of the electronic ground state of NO $X\ ^2\Pi_{1/2}$ was computed, using a Boltzmann distribution (with $T_{\rm rot}$ and $T_{\rm vib}$) to model the initial

TABLE III. Frequencies ($1/\alpha_{2\pi}\,\mathrm{ps}^{-2}$) for interference between pairs of paths for all possible paths that transport population from $|0,J'',m_J''\rangle$ to $|2,J,m_J\rangle$.

	$\|2,\frac{1}{2},\frac{1}{2}\rangle$	$\|2,1\frac{1}{2},\frac{1}{2}\rangle$	$\|2,1\frac{1}{2},1\frac{1}{2}\rangle$	$\|2,2\frac{1}{2},\frac{1}{2}\rangle$	$\|2,2\frac{1}{2},1\frac{1}{2}\rangle$	$\|2,2\frac{1}{2},2\frac{1}{2}\rangle$
O_{PP}-O_{2ph}	1.73	1.72	1.72	1.71	1.71	1.71
P_{QP}-P_{PQ}	1.58	2.63	2.63	3.67	3.67	3.67
P_{PQ}-P_{2ph}	3.09	3.73	3.73	4.44	4.44	4.44
P_{QP}-P_{2ph}	1.51	1.11	1.11	0.76	0.76	0.76
Q_{PR}-Q_{QQ}	1.86	3.41	3.41	5.21	5.21	5.21
Q_{PR}-Q_{RP}		4.71		7.06	7.06	
Q_{PR}-Q_{2ph}	4.10	5.65	5.65	7.45	7.45	7.45
Q_{QQ}-Q_{RP}		1.30		1.86	1.86	
Q_{QQ}-Q_{2ph}	2.24	2.24	2.24	2.24	2.24	2.24
Q_{RP}-Q_{2ph}		0.94		0.38	0.38	
R_{QR}-R_{RQ}		1.58		2.64	2.64	
R_{QR}-R_{2ph}		3.11		3.77	3.77	
R_{RQ}-R_{2ph}		1.53		1.13	1.13	
S_{RR}-S_{2ph}				1.76		

population distribution present in the molecular beam. In Fig. 7 the total populations in the vibrational states $v''=1$, 2, 3, and 4 are shown as a function of chirp for a laser pulse with $\nu=1845\,\mathrm{cm}^{-1}$, $\Delta\nu=50\,\mathrm{cm}^{-1}$, and a fluence of $\Phi=25\,\mathrm{mJ\,cm}^{-2}$. For the calculation a total of 45 states were used: $v''\in\{0,\ldots,4\}$, $J\in\{\frac{1}{2},\ldots,8\frac{1}{2}\}$, and m_J was restricted to $|m_J|\in\{\frac{1}{2},\ldots,J\}$. The calculation weighed the contribution of each initial state to the final states with the thermal population of that initial state. The thermal initial population was calculated for two different cases: (I) a Boltzmann distribution with $T_{\rm rot}=14\,\mathrm{K}$ and $T_{\rm vib}=1\,\mathrm{K}$, i.e., for only $v''=0$ as initial state, (II) same as (I); but now $T_{\rm vib}=300\,\mathrm{K}$ (see Table I) (circles in Fig. 7 at $\alpha=-1\times10^{-25}\,\mathrm{s}^2$).

The final-state population distribution is shown in Fig. 7 for both case (I) (dashed curves) and case (II) (solid curves). Note that the range of chirp for which the population is shown is now much smaller than for Fig. 5. The temperature values of case (II) represent the experimental conditions: $T_{\rm rot}$ is determined from the experiments in [17], and $T_{\rm vib}$ equals room temperature since no vibrational cooling in the supersonic expansion is assumed. The top panel shows that, for case (II), the population transfer to $v''=1$ by the IR laser is several times the thermally present population (indicated by the circles at $\alpha=-1\times10^{-25}\,\mathrm{s}^2$). As expected for the first excited state in a ladder system in the low intensity limit (no depletion of the $v''=0$ state), the population in $v''=1$ (top panel) only is a function of the fluence and *not* of the chirp. One panel down, the final population in $v''=2$ is displayed, which shows a strong enhancement for negative chirp, i.e., when the instantaneous frequency follows the consecutive steps up the vibrational ladder. For positive chirp the $v''=2$ population is expected to go to zero, since the molecule is irradiated with the required frequencies for transferring population from $v''=2\leftarrow1$ *before* the frequencies that transfer population from $v''=1\leftarrow0$. Consequently there would be no population in $v''=1$ that can be passed on to $v''=2$. This notion is confirmed by the prediction for case (I) (dashed curve). For case (II), however, there always is a nonzero population transfer to $v''=2$. This is attributed to transfer of

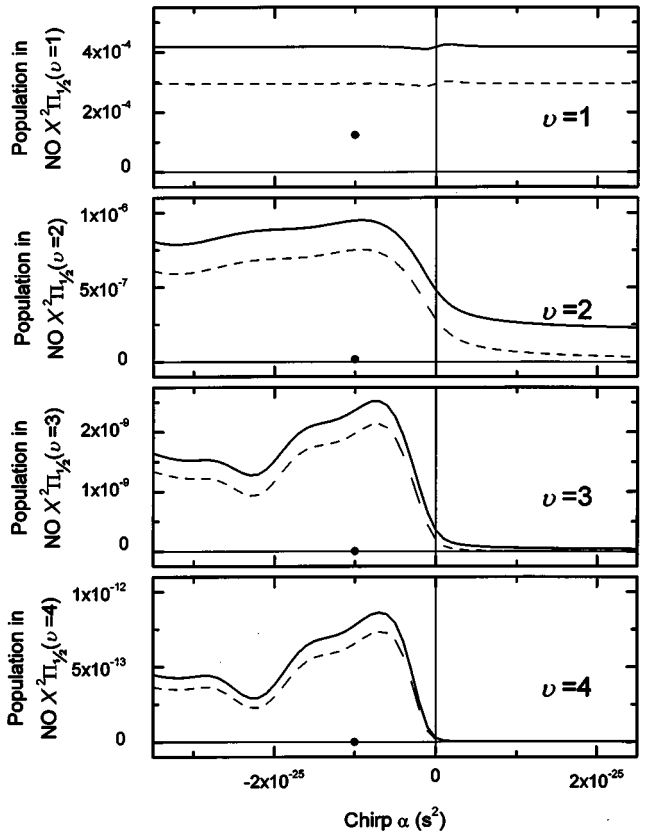

FIG. 7. The predicted population for, respectively, $v''=1$, 2, 3, and 4 as a function of the chirp, for a Gaussian laser pulse with $\nu_c=1845\,\mathrm{cm}^{-1}$ and $\Delta\nu=50\,\mathrm{cm}^{-1}$ for a pulse fluence of $\Phi=25\,\mathrm{mJ\,cm}^{-2}$. For the calculation nine rotational levels with all their m_J sublevels in five vibrational states of NO $X\,^2\Pi_{1/2}$ were included. The prediction for the final population distribution is calculated for an initial Boltzmann distribution of the population with (I) $T_{\mathrm{rot}}=14\,\mathrm{K}$ and $T_{\mathrm{vib}}=1\,\mathrm{K}$ (dashed curves) and for (II) $T_{\mathrm{rot}}=14\,\mathrm{K}$ and $T_{\mathrm{vib}}=300\,\mathrm{K}$ (solid curves). The circles at $\alpha=-1\times10^{-25}\,\mathrm{s}^2$ indicate the initial thermal population of the vibrational states for case (II) (see Table I).

population that is thermally present in $v''=1$. The weak oscillations in the dashed and solid curves for negative chirp show interference between several pathways. Here the interference mechanism which was introduced in the previous paragraphs is operative. The summing over all rotational states which are present in the beam causes the oscillations in the populations of individual rotational states to partially average out. Nevertheless the origin of the residual oscillations, both in theory and experiment, can be inferred.

Figure 8 displays the calculated $v''=2$ population as a function of the chirp for the individual $|2,J,m_J\rangle$ levels for $J\in\{\frac{1}{2},\ldots,2\frac{1}{2}\}$ along with the total population (solid curve, same data as in Fig. 7). This figure shows that under the experimental conditions the calculated population in $v=2$ is dominated by contributions $J''=\frac{1}{2}$, $m_J=\frac{1}{2}$, and $J''=\frac{3}{2}$, $m_J=\frac{1}{2}$. The observation that sublevels with $m_J=\frac{1}{2}$ are most efficiently excited to the $|2\rangle$ level persists in the calculations for higher vibrational states. This selection of $m_J=\frac{1}{2}$ sublevels means that the excited molecules become more aligned with the polarization direction of the IR laser with every step up on the vibrational ladder. These states were also included

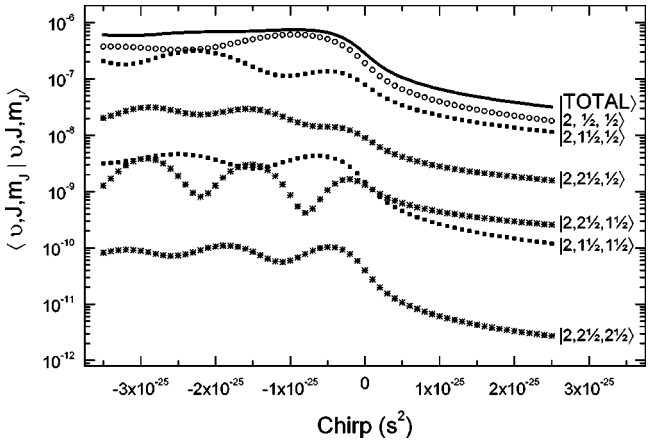

FIG. 8. The final population distribution over the states $|2,J,m_J\rangle$ as a function of the chirp, calculated for temperature case (I). The squares, circles, and diamonds denote the population in the states $|2,\frac{1}{2},m_J\rangle$, $|2,1\frac{1}{2},m_J\rangle$, and $|2,2\frac{1}{2},m_J\rangle$, respectively. Different values of m_J belonging to the same J are denoted by the same symbol, with m_J increasing from the top to the bottom data sets (i.e., the sublevel with $m_J=\frac{1}{2}$ is most efficiently populated for each J level). The total population in $|2\rangle$ is shown as a solid curve (and is identical the dashed curve shown in the second panel from the top in Fig. 7 [temperature case (I)]).

in the calculations in Fig. 6, and therefore we can now use the results of Fig. 6 to assess the interferences which give rise to the oscillations in the $v''=2$ population in the experiment. For excitation to $|v,J,m_J\rangle=|2,\frac{1}{2},\frac{1}{2}\rangle$ starting in $|0,\frac{1}{2},\frac{1}{2}\rangle$, the signal is originated by Q-type pathways, and an interference $Q_{PR}-Q_{QQ}$ takes place between a transition proceeding by a succession of an **R**- and a **P**-branch transition (i.e., via $|1,\frac{3}{2},\frac{1}{2}\rangle$) and a succession of two **Q**-branch transitions (i.e., via $|1,\frac{1}{2},\frac{1}{2}\rangle$. For excitation starting in $|0,\frac{3}{2},\frac{1}{2}\rangle$ the dominant signal arises from excitation to $|2,\frac{3}{2},\frac{1}{2}\rangle$, which is efficiently reached (i) by a succession of a **P** and **R** transition (i.e., via $|1,\frac{1}{2},\frac{1}{2}\rangle$, pathway Q_{PR}), (ii) by a succession of an **R** and **P** transition (i.e., via $|1,\frac{5}{2},\frac{1}{2}\rangle$, pathway Q_{RP}), and (iii) via a direct two-photon transition, pathway $Q_{2\mathrm{ph}}$. Two interferences between these pathways are identifiable in the calculations of Fig. 6 (middle panel), namely, interference $Q_{PR}-Q_{RP}$, between paths (i) and (ii) and interference $Q_{PR}-Q_{2\mathrm{ph}}$, between paths (ii) and (iii).

The lowest two panels of Fig. 7 show the population in $v''=3$ and $v''=4$ as a function of chirp. The curves have the same features as the curve for $v''=2$, but the interferences are more pronounced. This is due to the consecutive nature of the transfer up on the vibrational ladder: since both the distribution of the population over the rotational states and the interference periods $\alpha_{2\pi}$ do not change very much for the next steps up on the ladder, the transfer efficiency is enhanced (or reduced) for the same values of the chirp as for the transfer to $v''=2$. Hence the oscillatory structure in the transfer to intermediate vibrational states, as caused by the interference effects, is augmented as it is passed on to higher vibrational states.

C. Population transfer in the high-fluence limit

In the high-fluence limit the laser field is sufficiently strong to saturate the rovibrational transitions. For an elec-

tronic three-level ladder system in the rubidium atom it has been shown that, in the high-fluence limit, full transfer of the population from the ground to the top state by appropriate chirping of the laser pulse is possible [10], using the technique of rapid adiabatic passage [24,30]. For efficient chirped-pulse excitation of the HF molecule calculations are performed by Chelkowski and Bandrauk, including the effect of rotations [8]. In their paper an optimum in the transfer up the ladder as a function of the initial rotational state is observed for $J=5$, for negatively chirped laser pulses. Intuitively, one would expect maximum excitation for the lowest rotational states since they have the largest transition dipole moments. However, since the HF molecule has both a **P** and an **R** band connecting two vibrational states, population that is pumped up from $|v,J\rangle$ to $|v+1,J+1\rangle$ by an $R_{v+1,v}$ can subsequently become transferred down to $|v,J\rangle$ by the $\mathbf{P}_{v,v+1}$ resonance (pathway $Q_{\overline{PR}}$), before being excited to the next vibrational state $|v+2,J+2\rangle$ by the $\mathbf{R}_{v+2,v+1}$ transition (pathway S_{RR}). Thereafter, the molecule is no longer exposed to the frequencies required for pumping up to higher vibrational states. One can calculate the minimum rotational level for which the next step up ($\mathbf{R}_{v+2,v+1}$) always comes before a step down [either by $\mathbf{Q}_{v,v+1}$, for NO (the electronic ground state of NO is an intermediate coupling case between Hund's case *a* and *b*, allowing **Q** transitions for its lowest rotational states), or by $\mathbf{P}_{v,v+1}$, for NO and HF]. This demands that $\nu[\mathbf{P}_{v,v+1}(J)]<\nu[\mathbf{R}_{v+2,v+1}(J)]$. An estimate of these transition frequencies, made using the first two Dunham coefficients ω_e and $\omega_e x_e$ for the vibrational energy and B_e for the rotational energy, yields for $J_P>\omega_e x_e/(2B_e)$. Since **Q** transitions are allowed for the NO molecule, $\nu[\mathbf{Q}_{v,v+1}(J)]<\nu[\mathbf{R}_{v+2,v+1}(J)]$, or $J_Q>\omega_e x_e/(B_e)$. The above conditions yield for HF, with $\omega_e x_e=152\,\mathrm{cm}^{-1}$ and $B_e=21\,\mathrm{cm}^{-1}$, $J_P=4$, and for NO, with $\omega_e x_e=14.19\,\mathrm{cm}^{-1}$ and $B_e=1.7\,\mathrm{cm}^{-1}$, $J_P=4\frac{1}{2}$ and $J_Q=8\frac{1}{2}$ (the latter is not an additional restriction since *Q* transitions are already weak for $J\geqslant 4\frac{1}{2}$). So only rotational states with $J>J_P$ can become efficiently populated by a negatively chirped laser pulse. This explains why for HF the lowest rotational states, despite their largest transition dipole moments, are not most efficiently transferred to higher vibrational levels. For NO, in the low-fluence limit of the experiment, we have observed that the lowest states are most efficiently transferred, because of their largest transition dipole moment. Since for the lowest rotational states of NO **Q** transitions are allowed, it is possible to transfer consecutively up-down-up by the pathway $Q_{P\overline{QR}}$. This requires that $\nu[\mathbf{P}_{v,v-1}(J+1)]>\nu[\mathbf{R}_{v+1,v}(J)]$, or $J_{P\overline{QR}}<(\omega_e x_e-B_e)/2B_e$, or $J_{P\overline{QR}}\leqslant 3\frac{1}{2}$. Figure 3 shows that actually $J_{P\overline{QR}}\leqslant 2\frac{1}{2}$, which is probably due to neglect of the higher-order Dunham coefficients in the approximation of the transition frequencies. More importantly, the presence of the three resonances for the lowest three rotational states of the NO $X\ ^2\Pi_{1/2}$ state allows, in the high-fluence limit, efficient chirped-pulse excitation of highly excited vibrational states that are rotating very slowly, if rotating at all.

D. Comparison of calculations with experimental results

To compare the experimental data with the predicted population distributions, a simulated REMPI signal was calculated from the predicted population of state $|v,J,m_J\rangle$ by multiplying by the appropriate Hönl-London factors and 3-*J* symbols [27] for the NO $A\ ^2\Sigma(v')-X\ ^2\Pi_{1/2}(v'')$ transition. It was assumed that the ionization probability from the $A\ ^2\Sigma(v',J'')$ state is independent of the quantum numbers in the $A\ ^2\Sigma(v',J'')$ state [31]. The simulated REMPI signals from the individual states $|v,J,m_J\rangle$ were summed over the $\mathbf{Q}_{11}$ (for $J''\in\{\frac{1}{2},\ldots,4\frac{1}{2}\}$) and $\mathbf{P}_{21}$ branches (for $J''\in\{1\frac{1}{2},\ldots,4\frac{1}{2}\}$), yielding the calculated REMPI signal from the NO$(v',v'')\gamma$ band. Figure 1 displays both the measured and calculated REMPI signal (for $T_{\mathrm{vib}}=300\,\mathrm{K}$) as a function of the chirp. The *Y*-axis scaling is adjusted for each individual v''. The agreement between the simulation and the measurement is quite satisfactory. At $v=4$ the experimentally observed chirp dependence drops off considerably sharper than in the calculations, which is likely to be due to deviations in the wings of the spectrum of the FELIX IR pulse from our model Gaussian pulse. The importance of taking the thermal population in the higher vibrational states into account is illustrated by the agreement between experimental data and the simulation for $v''=2$, which both do not go to zero for $\alpha>0$ and $T_{\mathrm{vib}}=300\,\mathrm{K}$.

In the case of $v=2$, the analysis in the preceding section already provided a rationalization of the interference pathways which are responsible for the oscillations in the signal at negative chirp. For large negative values of α both the experiment and the theory show a reduction in the $v''=3$ and $v''=4$ population due to destructive interference between different rotational pathways. We have not attempted to assess which pathways are contributing most to the population transfer in this case, since for the basis sets required to compute the transfer to these high vibrational levels the calculations at large chirp became prohibitive.

VI. SUMMARY

In this article we have discussed results from experiments and model calculations on rotational interference in vibrational ladder climbing in the $X\ ^2\Pi_{1/2}$ state of NO. In the experiment the infrared pulses from a free electron laser (FEL) are frequency chirped. The populations in the vibrationally excited states of the electronic ground state of NO are probed with a 1+1 REMPI technique. For the one-photon process, driving population from $v=0$ to $v=1$, we found no significant dependence on the chirp, as expected. For the two-photon transition from $v=0$ to $v=2$ via $v=1$ the excitation was enhanced when the negative chirp of the laser pulse followed the negative anharmonicity of the vibrational ladder. However, the total population of $v=2$ showed an oscillatory behavior as a function of the applied chirp to the infrared laser pulse. These oscillations are attributed to interfering rotational pathways. With the help of the model calculations, the most relevant pathways resulting in the oscillations in the $v=2$ population are assigned. The oscillations in the $v=3$ and $v=4$ population, due to complex rotational interfering pathways, are found to be even more pronounced.

ACKNOWLEDGMENTS

It is a pleasure to acknowledge fruitful discussions with W. J. van der Zande and H. G. Muller, and the skillful as-

sistance by the FELIX staff, in particular, by A. F. G. van der Meer. This work is part of the research program of the Stichting Fundamental Onderzoek der Materie (FOM), which is financially supported by the Nederlandse Organisatie voor Wetenschappelijk Onderzoek (NWO).

APPENDIX: THE RELATION BETWEEN THE OSCILLATION PERIOD $\alpha_{2\pi}$ AND THE ENCLOSED AREA

For a Gaussian pulse with a rather large linear chirp α and central frequency ν_c, the instantaneous frequency at time t is given by [32]

$$\nu(t)=\nu_c+\frac{\pi}{\alpha}t. \tag{A1}$$

The phase difference between the contributions by the upper path I and lower path II is

$$\Delta\phi=\int_{t_1}^{t_2}(W_{\mathrm{I}}-W_{\mathrm{II}})dt, \tag{A2}$$

and, given the dressed-state eigenfrequencies $W_i(t)=E_i(t)/\hbar=2\pi[\nu_i+n_i\nu(t)]$:

$$\Delta\phi=2\pi\left[\int_{t_1}^{(t_1+t_2)/2}\nu_1+n\nu(t)-[\nu_0+(n+1)\nu(t)]dt+\int_{(t_1+t_2)/2}^{t_2}\nu_1+n\nu(t)-[\nu_2+(n-1)\nu(t)]dt\right]. \tag{A3}$$

One can easily see that only the relative photon number is of importance. Since the enclosed area has the shape of a right isosceles triangle (see Fig. 2), both integrals give equal contributions, thus

$$\Delta\phi=4\pi\int_{t_1}^{(t_1+t_2)/2}\nu_1-[\nu_0+\nu(t)]dt. \tag{A4}$$

For a strongly chirped Gaussian pulse, the instantaneous frequency is a linear function of time, so

$$\Delta\phi=4\alpha\int_{\nu_1-\nu_0}^{(\nu_2-\nu_0)/2}(\nu_1-\nu_0-\nu)d\nu, \tag{A5}$$

and, with the anharmonicity $\delta=(\nu_{21}-\nu_{10})\equiv[(\nu_2-\nu_1)-(\nu_1-\nu_0)]$,

$$\Delta\phi=\frac{\alpha}{2}\delta^2. \tag{A6}$$

For $\Delta\phi=2\pi$ the oscillation period $\alpha_{2\pi}$ is

$$\alpha_{2\pi}=\frac{4\pi}{\delta^2}. \tag{A7}$$

The enclosed area A in the dressed-level diagram is $A=(\delta/2)^2$, hence,

$$\alpha_{2\pi}=\frac{\pi}{A}. \tag{A8}$$

This expression is also valid for differently shaped enclosed areas. Equation (A8) may be used as long as the instantaneous frequency increases linearly in time, which is the case for a strongly chirped laser pulse (i.e., having a pulse duration that is at least three times larger than the transform limited pulse) with a Gaussian temporal profile.

[1] N. Bloembergen and E. Yablonovitch, Phys. Today **1978** (5), 23.
[2] P. A. Kwok *et al.*, Annu. Rev. Phys. Chem. **30**, 379 (1979).
[3] F. F. Crim, J. Phys. Chem. **100**, 12 725 (1996).
[4] R. D. F. Settle and T. R. Rizzo, J. Chem. Phys. **97**, 2823 (1992).
[5] S. A. Trushin, K. Sugawara, and H. Takeo, Chem. Phys. Lett. **267**, 573 (1997).
[6] S. Chelkowski, A. D. Bandrauk, and P. B. Corkum, Phys. Rev. Lett. **65**, 2355 (1990).
[7] S. Chelkowski and A. D. Bandrauk, Chem. Phys. Lett. **186**, 264 (1991).
[8] S. Chelkowski and A. D. Bandrauk, J. Chem. Phys. **99**, 4279 (1993).
[9] P. Balling, D. J. Maas, and L. D. Noordam, Phys. Rev. A **50**, 4276 (1994).
[10] D. J. Maas *et al.*, Phys. Rev. A **59**, 1374 (1999).
[11] R. J. Gordon and S. A. Rice, Annu. Rev. Phys. Chem. **48**, 601 (1997).
[12] V. V. Yakovlev *et al.*, J. Chem. Phys. **108**, 2309 (1998).
[13] A. Assion *et al.*, Chem. Phys. Lett. **259**, 488 (1996).
[14] S. Schiemann, A. Kuhn, S. Steuerwald, and K. Bergmann, Phys. Rev. Lett. **71**, 3637 (1993).
[15] A. Kuhn, S. Steuerwald, and K. Bergmann, Eur. Phys. J. D **1**, 57 (1998).
[16] V. D. Kleiman, S. M. Arrivo, E. J. Heilweil, and J. S. Melinger, Chem. Phys. **233**, 207 (1998).
[17] D. J. Maas, D. I. Duncan, R. B. Vrijen, W. J. van der Zande, and L. D. Noordam, Chem. Phys. Lett. **290**, 75 (1998).
[18] J. S. Melinger *et al.*, J. Chem. Phys. **101**, 6439 (1994).
[19] D. Oepts, A. F. G. van der Meer, and P. W. van Amersfoort, Infrared Phys. Technol. **36**, 297 (1995).
[20] G. M. H. Knippels *et al.*, Opt. Commun. **118**, 546 (1995).
[21] D. C. Jacobs and R. N. Zare, J. Chem. Phys. **85**, 5457 (1986).
[22] D. C. Jacobs, R. J. Madix, and R. N. Zare, J. Chem. Phys. **85**, 5469 (1986).
[23] G. Herzberg, *Molecular Spectra and Molecular Structure*, 2nd ed., Spectra of Diatomic Molecules. Vol. I (Van Nostrand Reinhold Company, New York, 1966).
[24] E. C. G. Stueckelberg, Helv. Phys. Acta **5**, 369 (1932).
[25] F. A. Jenkins, J. Opt. Soc. Am. **43**, 425 (1953).
[26] R. Engleman, Jr., P. E. Rouse, H. M. Peek, and V. D. Baia-

monte, Los Alamos Scientific Laboratory Report No. LA-4364, 1970.
[27] R. N. Zare, *Angular Momentum. Understanding Spatial Effects in Chemistry and Physics* (John Wiley & Sons, Inc., New York, 1988).
[28] T. W. B. Kibble, Phys. Rev. **150**, 1060 (1966).
[29] A. V. Oppenheim, A. S. Willsky, and I. T. Young, *Signals and Systems* (Prentice-Hall, London, 1983).
[30] R. B. Vrijen, G. M. Lankhuijzen, D. J. Maas, and L. D. Noordam, Comments At. Mol. Phys. **33**, 6 (1996).
[31] H. Zacharias, F. de Rougemont, T. F. Heinz, and M. M. T. Loy, J. Chem. Phys. **105**, 111 (1996).
[32] A. E. Siegman, *Lasers* (University Science Books, Mill Valley, CA, 1986).